Integrating distributed acoustic sensing, borehole 3C geophone array, and surface seismic array data to identify long-period long-duration seismic events during stimulation of a Marcellus Shale gas reservoir

Payam Kavousi Ghahfarokhi[1], Thomas H. Wilson[1], Timothy Robert Carr[1], Abhash Kumar[2], Richard Hammack[2], and Haibin Di[3]

Abstract

Microseismic monitoring by downhole geophones, surface seismic, fiber-optic distributed acoustic sensing (DAS), and distributed temperature sensing (DTS) observations were made during the hydraulic fracture stimulation of the MIP-3H well in the Marcellus Shale in northern West Virginia. DAS and DTS data measure the fiber strain and temperature, respectively, along a fiber-optic cable cemented behind the casing of the well. The presence of long-period long-duration (LPLD) events is evaluated in the borehole geophones, DAS data, and surface seismic data of one of the MIP-3H stimulated stages. LPLD events are generally overlooked during the conventional processing of microseismic data, but they represent significant nonbrittle deformation produced during hydraulic fracture stimulation. In a single stage that was examined, 160 preexisting fractures and two faults of suboptimal orientation are noted in the image logs. We identified two low-frequency (<10 Hz) events of large temporal duration (tens of seconds) by comparing the surface seismic data, borehole geophone data, and DAS amplitude spectra of one of the MIP-3H stages. Spectrograms of DAS traces in time and depth reveal that the first low-frequency event might be an injection noise that has footprints on all DAS channels above the stimulated stage. However, the surface seismic array indicates an LPLD event concurrent with the first low-frequency event on DAS. The second LPLD event on DAS data and surface seismic data is related to a local deformation and does not have footprints on all DAS channels. The interpreted events have duration less than 100 s with frequencies concentrated below 10 Hz, and are accompanied by microseismic events.

Introduction

Hydraulic fracturing of unconventional shale reservoirs is necessary to enhance the reservoir permeability. Hydraulic fracturing has been undertaken by various operators since the 1940s (Montgomery and Smith, 2010). Companies carry out a multistage perforation followed by a high-pressure fluid/proppant slurry injection to create long hydraulic fractures within low-permeability reservoirs. These hydraulic fractures combined with significant stimulation of the bounding natural fracture network increase the stimulated reservoir volume and subsequent reservoir production. The present-day stress orientation within the reservoir exerts the greatest influence on the direction of hydraulic fracture growth. However, the density, orientation, and openness of natural fractures/faults can also affect the direction and complexity of hydraulic fracture propagation.

Brittle failure along preexisting fractures generates small-magnitude microseismic events (MSEs) as high-frequency seismic waveforms with clear P- and S-arrivals. These MSEs are interpreted to result from shear slip on preexisting fractures and faults near induced hydraulic fractures (Rutledge and Phillips, 2003; Warpinski et al., 2004; Das and Zoback, 2013a). Although microseismicity is used as a direct measure to calculate the stimulated reservoir volume, the correlation is debatable (Sicking et al., 2012; Wilson et al., 2016). Energy balance between MSEs and injection energy has been compared in several studies (Boroumand and Eaton, 2012; Warpinski et al., 2012; Kavousi et al., 2017; Kumar et al., 2017b). Results show that the energy released in the form of MSEs is only a small portion of the energy supplied to the reservoir during hydraulic fracture stimulation as estimated from treatment pressure and injection volume. This deficit suggests that energy release by other deformation mechanisms are important components of the input-output energy balance associated with hydraulic fracturing. Recently, long-period long-duration (LPLD) events have been considered to be a potential source for energy consumption by slow shear slip on relatively large faults (Das and Zoback, 2011, 2013a; Mitchell et al., 2013; Kwietniak, 2015). Das and Zoback (2013a) show that LPLD events release 1–2 orders of magnitude more en-

[1]West Virginia University, Morgantown, West Virginia, USA. E-mail: pkavousi@mail.wvu.edu; tom.wilson@mail.wvu.edu; tim.carr@mail.wvu.edu.
[2]NETL DOE, Pittsburgh, Pennsylvania, USA. E-mail: abhash.kumar@netl.doe.gov; richard.hammack@netl.doe.gov.
[3]Georgia Tech University, Atlanta, Georgia, USA. E-mail: haibin.di@ece.gatech.edu.

ergy than observed MSEs and may contribute much more to reservoir stimulation than that associated with observed microseismicity. Zoback et al. (2012) show that fracture and fault orientations relative to the present-day SH_{max} could determine the slip behavior. They propose through modeling that misaligned faults undergo slow slip, whereas well-oriented faults and fractures undergo brittle failure in response to increased fluid pressure. The reason might be that fluid pressure propagates faster along well-oriented faults than misaligned faults and triggers a rapid slip. Das and Zoback (2013a) suggest that LPLD events result from slow shear slip on preexisting faults that are unfavorably oriented in the present-day stress field or have high clay content.

Das and Zoback (2011) analyze borehole seismic data from hydraulic fracturing in the Barnett Shale. They interpret the LPLD events as a low-frequency energy release (between 10 and 80 Hz) that lasts from tens of seconds to minutes. The LPLD events are usually characterized by low-amplitude arrivals and incoherent phase, making the phase picking very difficult (Das and Zoback, 2011; Eaton et al., 2013). LPLD seismic events have similarities with observed tectonic tremors in subduction zones and transform faults (Caffagni et al., 2015). Tectonic tremors are assumed to be accompanied by slow shear slip of plates in transform faults or subduction zones (Obara, 2002; Shelly et al., 2006; Nadeau and Guilhem, 2009). Das and Zoback (2011) suggest that similar phenomena could happen during hydraulic fracturing when there is slow slip on preexisting faults of suboptimal orientation. They propose that this nonbrittle deformation process could contribute to reservoir production by significant permeability enhancement. Mitchell et al. (2013) analyze the seismic waveforms from surface and downhole geophone arrays during hydraulic fracturing of a horizontal well in the Cline Shale of West Texas to detect LPLDs. The spectrogram of the stacked waveforms from the downhole array revealed the presence of several LPLDs; however, no LPLDs were detected in the surface recordings, most likely because of low signal strength. Eaton et al. (2013) study seismic waveforms recorded during the hydraulic fracturing of a well in a Montney gas reservoir in British Colombia and identify several LPLD events. They observe LPLD events at frequencies less than 10 Hz and propose that complexity of preexisting natural fractures could affect the spectral frequency of LPLD events. Analysis of distributed acoustic sensing (DAS) data requires that fiber distortions and regional tectonic events unrelated to the local reservoir response be ruled out as possible LPLD events. Recently, Caffagni et al. (2015) and Zecevic et al. (2016) point out that the regional seismic events can be misidentified as LPLD events due to their similar waveform characteristics, overlapping frequency content, and apparent velocity. For regional earthquakes, codas of P- and S-waves that are multiply reflected and scattered may also produce the effect of long-duration signals with ambiguous arrival times similar to LPLD events (Aki, 1969; Aki and Chouet, 1975). In the recent past, Kumar et al. (2017a, 2018) identify several LPLDs in the surface seismic data recorded during hydraulic fracturing of the Marcellus Shale wells at the current study site in Monongalia County, West Virginia. To avoid any misinterpretation between an LPLD event and known or unknown regional earthquakes, Kumar et al. (2017a, 2018) analyze seismic waveforms from the nearest stations of the USArray and cross-checked regional earthquakes. Kumar et al. (2017a, 2018) find that no temporal correlation between the LPLD events detected from surface broadband stations and known catalog events, suggesting a local source of deformation as the cause of the LPLD events.

The absence of regional earthquake activity during stimulation allows us to explore the DAS and distributed temperature sensing (DTS) data for possible LPLD events associated with hydraulic fracturing of a horizontal Marcellus Shale well in Monongalia County of West Virginia. Fiber-optic DAS and DTS data record the strain or strain rate and temperature around the wellbore, respectively. Fiber-optic sensing technology has been used by oil and gas companies since 1990s to monitor steam injection, injection profiling, acid injection profiling, and hydraulic fracture diagnostics (Karaman et al., 1996; Sierra et al., 2008; Glasbergen et al., 2010; Rahman et al., 2011; Holley and Kalia, 2015). DAS is sensitive to the vibrations in the local environment around the fiber, and it provides a measure of the relative axial strain or strain rate of the optical fiber (Tanimola and Hill, 2009).

The frequency content of DAS data has been studied by several researchers. Ghahfarokhi et al. (2018) show that seismic attributes, such as instantaneous frequency, dominant frequency, and energy, could be applied to DAS data to better monitor hydraulic fracturing. Jin and Roy (2017) show that very low-frequency strain-rate DAS signals could reveal information about the stress shadow, fracture length, density, and width. However, low-frequency DAS data can be significantly affected by temperature variations around the fiber during cross-stage flow communications. Elimination of this effect requires fiber cable installation in a separate monitoring well rather than the stimulated well.

DAS fiber-optic data have also been used to detect MSEs with high accuracy (Webster et al., 2016). Karrenbach et al. (2017) use DAS data to locate MSEs with accuracy similar to locations obtained from sensors deployed in the monitoring well. A field trial of vertical seismic profiling (VSP) by DAS fiber-optic was conducted at the Aquistore site in Saskatchewan, Canada. Olofsson and Martinez (2017) show that the VSPs from processed DAS fiber-optic data of three different vendors are similar to VSP data recorded by conventional geophone arrays.

In this study, we analyze borehole geophone data and DAS data collected during stimulation of the MIP-3H well close to Morgantown, West Virginia (Figure 1). The DAS data were recorded in fiber deployed along the length of

the MIP-3H horizontal well, and the borehole seismic data were recorded by geophones deployed in a vertical monitoring well MIP-SW (Figure 1). Figure 1 also shows five surface seismometers of which FRAC3 and FRAC4 were operating intermittently during hydraulic fracturing due to power shortage.

We propose that a frequency spectrogram of fiber-optic DAS data could show LPLD events concurrently with surface seismic array in low frequencies. We also examine the possibility that temperature variation might be observed simultaneously with LPLD events on DTS data as a result of hydraulic connections through fractures and faults. It is very unlikely that regional earthquakes can alter the temperature around the fiber. So, the combined analysis of fiber-optic DAS and DTS can be used to differentiate LPLD events produced by stimulation and those produced by regional earthquakes.

Data sets and methodology

In 2015, two horizontal wells, MIP-3H and MIP-5H, were hydraulically fractured in the Marcellus Shale close to Morgantown (Figure 1), West Virginia, in the eastern United States. The lateral of the MIP-3H well is drilled just above the Cherry Valley Limestone in the Upper Marcellus Shale. A permanent fiber-optic cable was deployed in the MIP-3H well to acquire DAS and DTS data throughout the stimulation of all 28 stages along this well. A total of 493 DAS channels recorded vibrations along the lateral with a spacing of approximately 16.74 ft (5.1 m) and a gauge length of 64 ft. DTS data were recorded with a higher resolution of approximately 1 ft (30.48 cm) during hydraulic fracture stimulation. In addition, microseismic activity during hydraulic fracturing was monitored by the vertical MIP-SW well, which had 12 3C geophones separated by 100 ft (30.48 m) interval (Figure 2). The total vertical aperture of the geophone array was 1100 ft (335.28 m).

The focus of this study is to integrate DAS, DTS, surface seismic, and borehole seismic data from the MIP-3H well stimulation and inspect these data for potential LPLD events. We compute the spectrogram of geophone channels deployed in the vertical well and compare them with the spectrogram of the DAS channels for stage 10 to detect LPLD events. We then analyze surface seismic data to evaluate if the LPLDs are recorded on the surface array. Stage 10 is chosen for this study because it has the most preexisting fractures and faults among the 28 stages. Interpretation of the formation image log by an independent contractor along the length of the lateral identified two faults and 160 preexisting fractures across the length of stage 10. The natural fracture intensity across this stage exceeds that across other stages. The faults and high natural fracture intensity along stage 10, complemented by the high clay content of the Marcellus Shale, could facilitate the generation of LPLD events through slow slip. We evaluate the DAS, DTS, surface seismic, and borehole geophone data from the stage 10 stimulation for the presence of LPLD events.

Figure 1. The MSEEL site just outside Morgantown, West Virginia, USA. The MSEEL site consists of four horizontal production wells operated by Northeast Natural Energy LLC (MIP-3H, MIP-4H, MIP-5H, and MIP-6H), two pilot holes (MIP-3 and MIP-4), a microseismic observation well (MIP-SW), and a grid of five surface seismometers (triangles). FRAC3 and FRAC4 were working intermittently during hydraulic fracturing due to a limited power supply. The location of the studied stage 10 is also shown on well MIP-3H.

Discussions and results

Ghahfarokhi et al. (2018) evaluate the DTS (Figure 3a) and DAS data of the stage 10 stimulation for well 3H for the presence of low-frequency time intervals in the DAS data. The instantaneous frequency attribute (Figure 3b) was calculated from a Hilbert transform of the DAS signals from stage 10 stimulation. They pro-

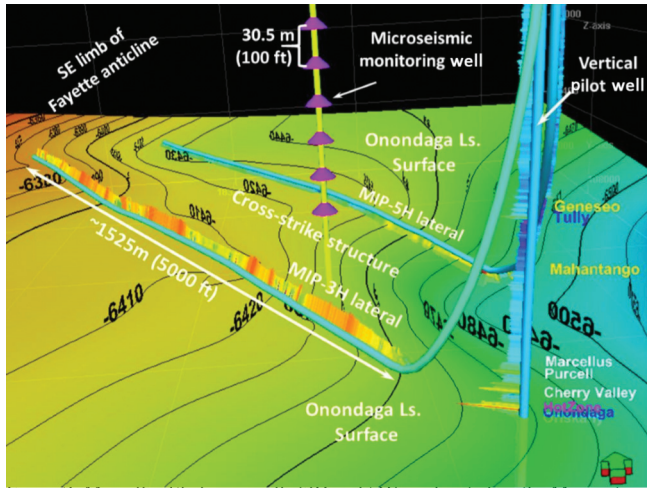

Figure 2. Three-dimensional view of wells located in the study area. DAS data were collected in the MIP-3H. Contours on the top of the Onondaga Limestone (base of the Marcellus Shale) are in feet subsea. Gamma-ray log responses are shown in the vertical pilot well and the two horizontal wells. Geophone locations are shown in the lower part of the microseismic monitoring well.

pose that the temperature rise observed in stage 9 (Figure 3a) during stimulation of stage 10 resulted from fluid communication through preexisting faults and fractures. The fluid from stage 9 stimulation remained in the formation fractures for several hours and reached the reservoir temperature of approximately 160°F. Stage 10 stimulation likely pushed back the warmed fluid toward stage 9 through cross-stage fractures that resulted in warming as observed on the DTS data. Jin and Roy (2017) suggest that temperature variations could affect the low-frequency components of DAS data. The effect of the temperature was filtered by the service company during the recording of the DAS data. Figure 3b shows low-frequency intervals that are in the vicinity of the abnormal temperature. We observed that the low-frequency (<10 Hz) time intervals in Figure 3b are also concurrent with increased microseismic activity recorded at the downhole geophones in the monitoring well (Figure 3c). MSEs were also recorded during the leakoff period and are concurrent with the low instantaneous frequency in the DAS data.

Independent interpretation of the formation image log shows two faults and 160 fractures for stage 10. The natural fractures in this area have average orientation of approximately N83°E along with the faults at the N30°E orientation. Wilson et al. (2018) analyze the formation image logs of the MIP-3H well and report a present-day SH_{max} orientation of N57°E based on the orientation of induced fractures observed in the vertical pilot well. Given this orientation of current SH_{max}, the fractures and faults detected in stage 10 are roughly at 26° east of the SH_{max} and 27° north of the SH_{max}, respectively. As suggested by Fisher and Guest (2011), tensile failure could happen for preexisting natural fractures with an orientation of less than or equal 10° relative to the SH_{max} direction. Natural fractures and faults that are oriented at higher angels to SH_{max} most likely experience shear failure when subjected to increased pore pressure conditions (Das and Zoback, 2013b). Wilson et al. (2018) suggest that most of the natural fractures across this stage will experience shear failure with increased pore pressure during hydraulic fracture treatment. In addition, the high clay content of the Marcellus Shale could facilitate a slow shear slip on the preexisting faults and fractures during the stimulation of the associated stage.

The spectrum of the microseismic data (Figure 4) was computed for a data set consisting of the sum of the z-component response for all 12 geophones in the monitoring well array. The 0.0005 s sample interval equals that of the DAS data. A relatively high-amplitude low-frequency response is observed in two time intervals that extend from approximately 2500 to 3200 s and 6900 to 7300 s. The first low-frequency interval, observed near 3000 s, is simultaneous with formation breakdown. Spectra of the x- and y-components did not resolve low-frequency intervals as well as for the z-component.

We evaluated a DAS channel 50 ft (15 m) away from stage 10, which is in the top of stage 9 (Figure 5a), against the sum of the 10–80 Hz filtered z-component amplitudes of the borehole geophones recorded during the stimulation of stage 10 (Figure 5b). The DAS data are low-pass filtered at an 80 Hz frequency. The filtered spectrogram of the DAS channel from stage 9 (Figure 5a) reveals low-frequency intervals that can also be seen on the 10–80 Hz filtered microseismic data at higher frequencies. DAS and borehole geophones record the same seismic wavefields, but they may have different types of noise. The discrepancy of frequency contents between spectrogram of DAS data and borehole geophone data could suggest that the DAS signal-to-noise ratio is too low to record microseismic data at high frequencies. However, borehole geophones in the microseismic monitoring well have limitations in recording frequencies less than 10 Hz. Figure 5b

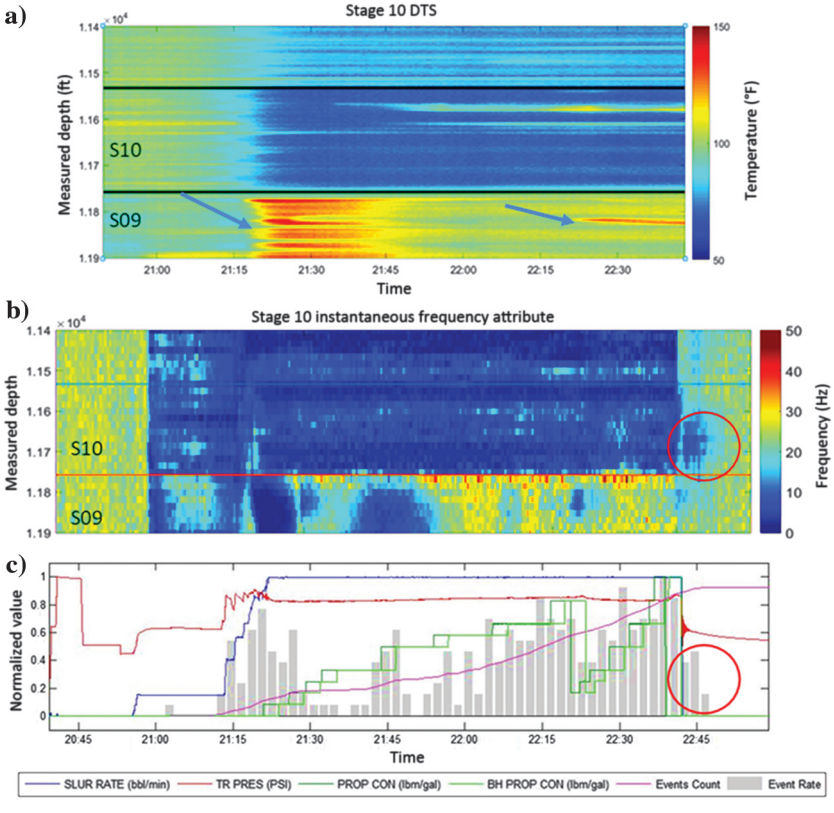

Figure 3. (a) The DTS data for stimulation of stage 10. The warmer color (arrows) shows higher temperature in stage 9. (b) The DAS instantaneous frequency attribute reveals low-frequency time intervals in stage 9 (S09) during stimulation of stage 10. Note the leakoff period marked by a circle. (c) Normalized pumping data of the stage 10 stimulation are shown. The bar histogram shows the MSEs recorded in the borehole geophones of the monitoring well. The circle shows the microseismic activities during the leakoff period.

shows that the low-frequency feature approximately 4200 s in DAS data is not evident on the spectrogram of the stacked z-component geophones.

The DAS low-frequency events at approximately 3000, 4500, and 7000 s appear to be too slow for regular borehole geophones to record. However, these low-frequency events on DAS data are associated with microseismic activity that is recorded by geophones. The persistent very long-duration low-frequency (10–30 Hz) signal between 2500 and 8000 s on the geophones' spectrogram (Figure 5b) appears to be related to coupling of pumping induced vibrations into the subsurface. Eaton et al. (2013) notice similar low-frequency features that persist for an entire stage stimulation. Das and Zoback (2013a, 2013b) also mention that transport of the treatment fluids inside the pipe might induce oscillations in the formation and cause an LPLD-like frequency response on microseismic spectrogram. Figure 5 also shows persistent frequency strips at approximately 30 and 60 Hz that could be noises picked by the DAS interrogator at the surface and geophones in the monitoring well.

We inspected data collected from the downhole microseismic geophone array during stage 10 stimulation to understand the low-frequency intervals (10–80 Hz). The downhole geophone data in Figure 6a show that many MSEs are recorded as spikes in the 10–80 Hz data at approximately 3000, 4000, and 7000 s. The event at approximately 7000 s does not show significant amplitude variations with depth. Figure 6b shows a 2 s window at approximately 7000 s event. There are many other events like Figure 6b at approximately 7000 s that have a moveout toward the deepest geophone. A moveout toward the reservoir reveals that the moveouts of events within this zone have a source above the geophone array and are not related to deformation associated with stage 10 stimulation.

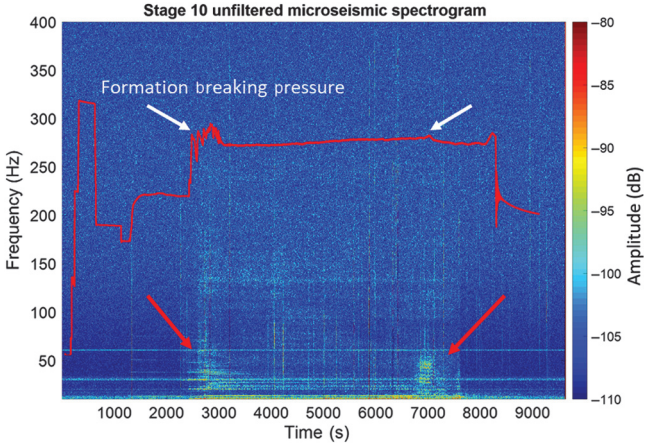

Figure 4. The raw unfiltered microseismic spectrogram of the average z-component observed during stage 10 stimulation. The red curve shows the normalized treatment pressure. Low-frequency time intervals are during the initial period of high treatment pressure and during another smaller pressure increase.

We also looked at the surface seismic data recorded by the local broadband seismometer network at approximately 7000 s. Figure 7a–7c shows that this event was strongest at FRAC1 and decays with distance away from the pad toward FRAC2 at approximately 1.6 km from FRAC1 and FRAC5 at approximately 4.6 km from FRAC1. The FRAC1 seismometer is very close to the wellpad (See Figure 1). This observation at the surface seismometers and downward moveout on geophone data (Figure 6b) suggests that this event is not related to downhole deformation and has its source close to the wellpad.

We then band-pass filtered the DAS data to frequencies between 0.1 and 5 Hz to show the low-frequency events at approximately 3000 and 4500 s identified from the DAS spectrogram in Figure 5a. Figure 8a shows that these low-frequency events on DAS data are concurrent with increased MSE count in Figure 8b. It also shows that injection noise is apparent in all the DAS data at approximately 3000 s. This observation casts doubt on the hypothesis that this event is an LPLD event. Fracturing fluid movement inside the casing is also evident from 1800 to 2000 s with an apparent velocity of 9 ft/s.

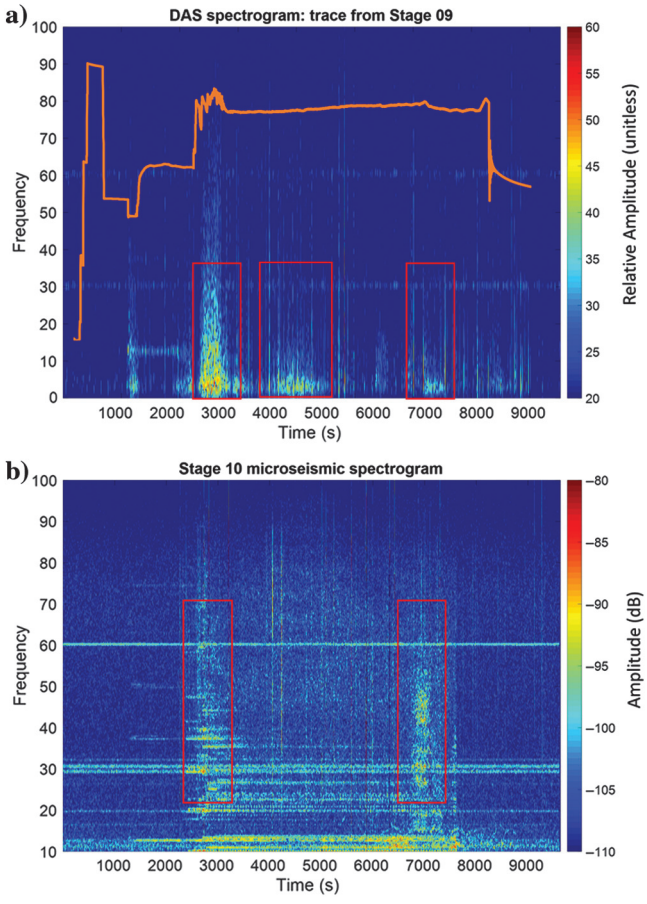

Figure 5. (a) Stage 10 stimulation low-frequency time intervals in DAS trace 371, which is in stage 9. The orange curve shows the treatment pressure. The DAS data are 80 Hz low-pass filtered. (b) Spectrogram of sum of the 10–80 Hz band-pass filtered z-components of stage 10 microseismic. Note that DAS events are lower than low-frequency intervals in geophone data.

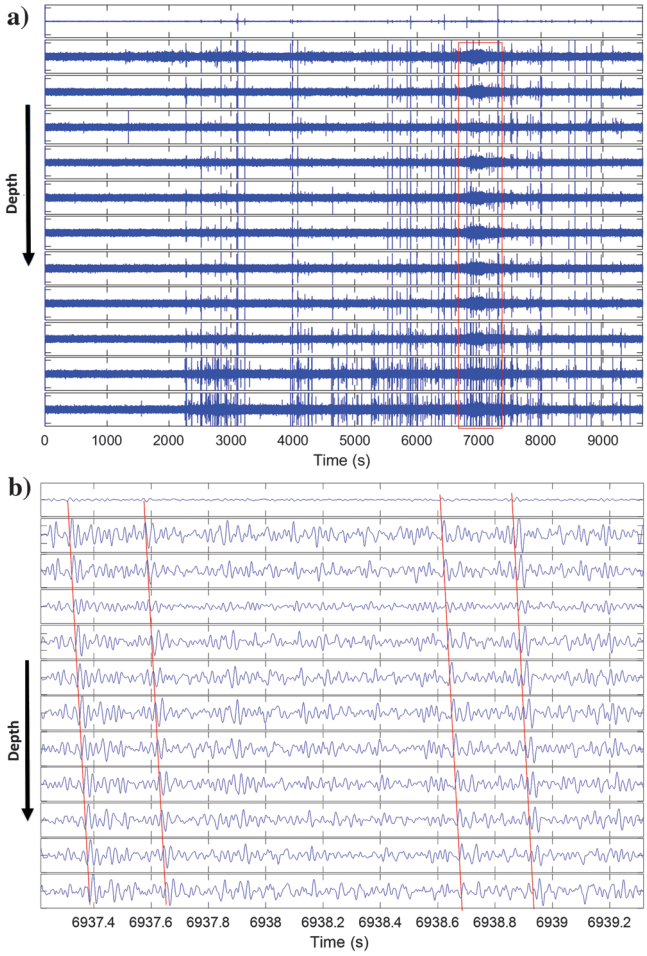

Figure 6. (a) The 10–80 Hz filtered z-components of 12 downhole geophones are shown. Note the features at approximately 3000, 4000, and 7000 s. (b) Many of the events in the highlighted time interval approximately 7000 s in Figure 6a display moveout similar to that shown for this 2 s interval.

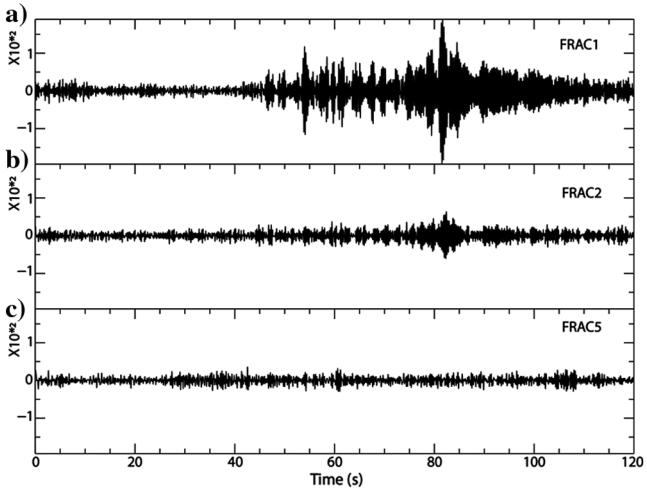

Figure 7. The surface seismometer recorded seismic activities at approximately 7000 s. (a) The FRAC1 seismometer is close to the wellpad, (b) FRAC2 seismometer, and (c) FRAC5 seismometer.

The first low-frequency interval at approximately 3000 s appears (Figure 8a) to be affected by injection noise. The event at approximately 4200 s is also concurrent with increased microseismic activity. This feature is likely to be related to local deformation, and it is not visible on all DAS channels. Figure 8b also reveals that many MSEs occurred close to 8000 s. However, the DAS data do not show them. The noise-like 7000 s events in microseismic z-component are also not visible on the low-frequency DAS data in Figure 8a.

The spectrograms of 0.1–5 Hz low-pass-filtered DAS channels are shown in Figure 9 for every 10 traces along the well. Twenty-four spectrograms of DAS traces are plotted over each other in a waterfall plot to reveal frequency variations in time and depth. The waterfall plot of spectrograms is comparable to filtered DAS data in Figure 8a. The event at approximately 3000 s appears to have the maximum amplitude in stage 10 and attenuates as it goes toward the toe of the well (higher measured depth). However, the footprint of this event is apparent on all shallower DAS channels. This could be due to injection noise. Stage 10 is separated by plugs from stage 9 to stage 1. The moveout in Figure 8a is also identifiable in Figure 9. This moveout is most likely related to the movement of slurry along the length of the casing. The observations presented in Figures 8 and 9 cast doubts on the interpretation of the 3000 s event as an LPLD event.

However, surface seismic arrays recorded a seismic event at approximately 3000 s with 20–30 s duration (Figure 10). This low-frequency event (0.8–3 Hz) was ob-

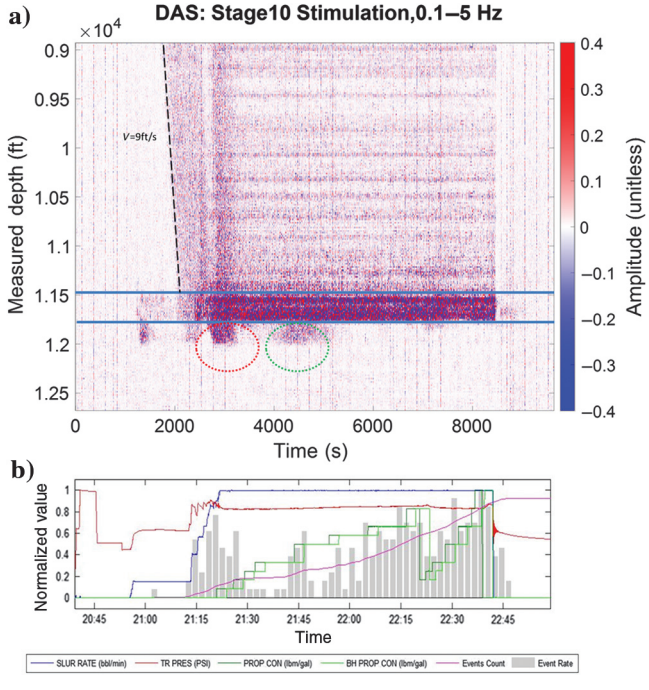

Figure 8. (a) The DAS data are band-pass filtered between 0.1 and 5 Hz. (b) Normalized pumping data of the stage 10 stimulation are shown. The bar histogram shows the MSEs recorded in the borehole geophones of the monitoring well.

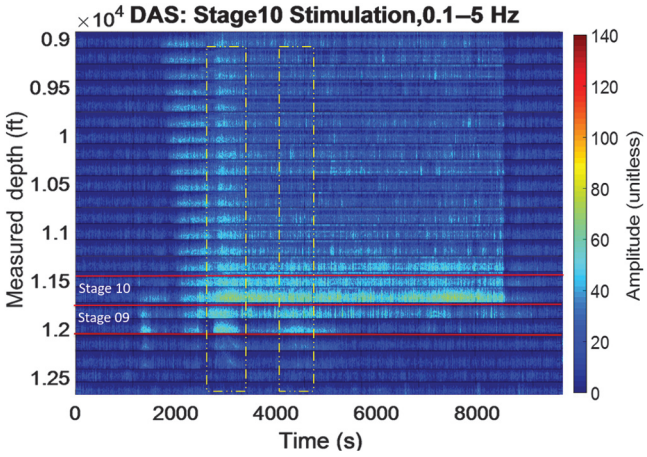

Figure 9. The spectrograms of DAS traces observed along the length of the lateral reveal variations of frequency through time and measured depth. All spectrograms are from filtered DAS data between 0.1 and 5 Hz shown in Figure 8a. Events at approximately 3000 and 4200 s are enclosed within rectangles.

served in three of the surface seismometers (Figure 10a). The seismometers FRAC1, FRAC2, and FRAC5 are located at distances of approximately 3.1, 2.1, and 3 km, respectively, from stage 10. Using an average velocity of 4.4 km/s, the relative differences in traveltimes from stage 10 to the seismometer surface locations are less than approximately 0.23 s. These records were stacked (Figure 10b), and their combined spectrum (Figure 10c) reveals high amplitudes for frequencies between approximately 1 and 4 Hz. High-amplitude events at this approximate time are also observed in the deeper microseismic sensors in the monitoring well. These events (Figure 10b) are interpreted as LPLD events.

MSEs are also observed in the monitoring well in the deeper sensors at approximately 4200 s (Figure 6a). A long-duration disturbance is also observed at this time in the DAS data in stage 9 (Figures 8 and 9). Unlike the 3000 s event, this 4200 s event is not visible on all DAS channels and is restricted to stage 9. This low-frequency interval attenuates from stage 10 toward the heel and

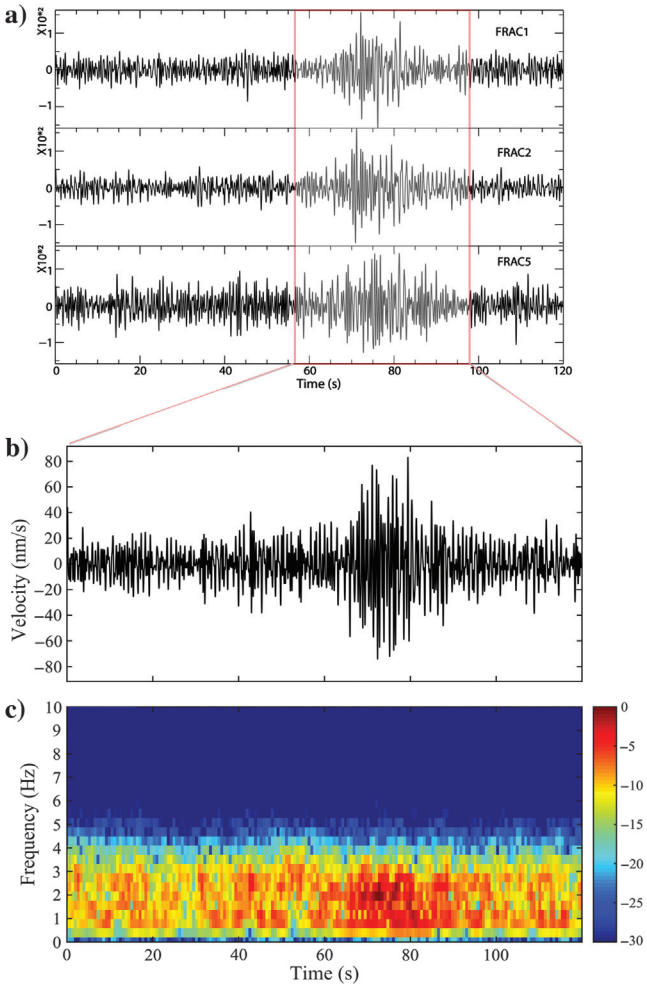

Figure 10. (a) The seismic event at approximately 3000 s is recorded by all surface seismometers. (b) Stacked waveforms of the three seismometers. Stacking is done after filtering the individual waveforms recorded at FRAC1, FRAC2, and FRAC5 in the frequency range of 0.8–3 Hz. (c) Spectrogram of the final stacked waveform.

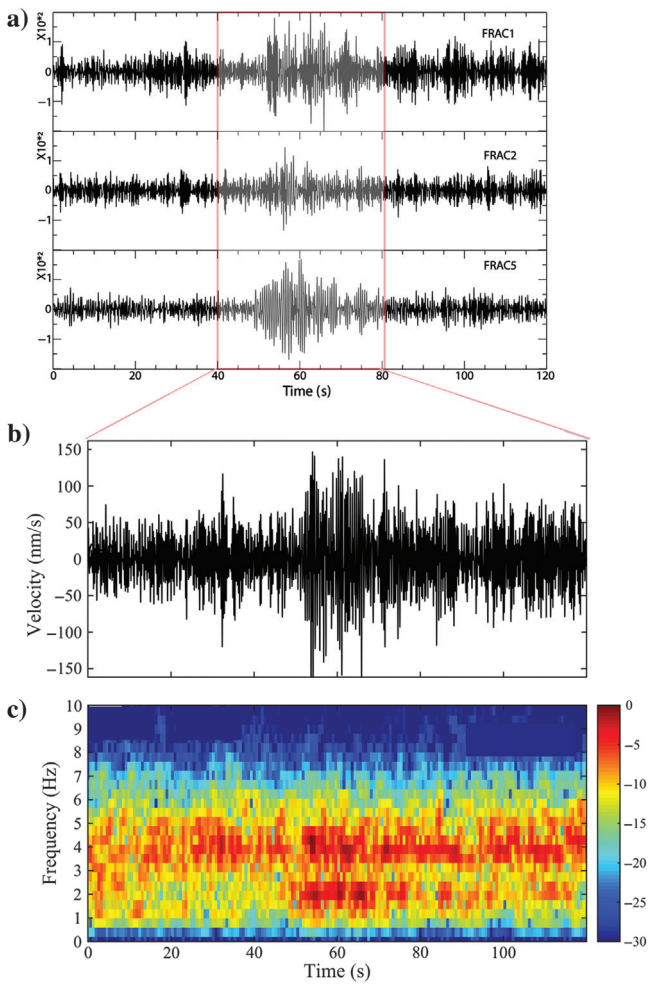

Figure 11. (a) The seismic event at approximately 4200 s is recorded by all surface seismometers. (b) Stacked waveforms of the three seismometer. Stacking is done after filtering individual waveforms recorded at FRAC1, FRAC2, and FRAC5 in the frequency range of 0.8–3 Hz. (c) Spectrogram of the final stacked waveform.

toe of the well. Figure 11 shows that the surface seismic array recorded an event at approximately 4200 s in all three seismometers.

The interpreted LPLD events from DAS and surface seismic in this study have lower frequency content (in the range of <10 Hz) than LPLDs from the Barnett Shale interpreted by Das and Zoback (2013a, 2013b). Eaton et al. (2013) propose that the fracture network complexity could affect the dominant frequency content of LPLD events. They interpret LPLD events from the Montney Shale (British Columbia) with frequencies of less than 10 Hz. The lower observed frequency of LPLD events in the Montney Formation, compared to the Barnett Shale, was attributed to the less complex fracture network in the Montney Formation (a single fracture set). Fisher et al. (2005) categorize the Barnett Shale as a formation with a very complex fracture network consisting of two intersecting fracture sets: a northeast–southwest set and another northwest–southeast set. Formation image logs of the MIP-3H vertical well reveal the presence of two fracture sets with orientations of N87°E and N57°E, whereas those observed in the horizontal well fell mostly in a single set with average orientation of N83°E (Wilson et al., 2018). Our observations from the surface seismic, DAS, and borehole microseismic reveal that LPLD events in stage 10 have frequencies less than 10 Hz similar to frequency range of LPLD events of the Montney Formation.

Conclusion

Our analysis of the DAS, downhole geophone data, and surface seismic data of stage 10 brings the following concluding remarks:

- Spectrograms of the DAS and borehole geophone data reveal different frequency content. The DAS spectrogram showed lower frequency content than the borehole geophone data. This unusual finding is attributed to the poor signal-to-noise ratio for the DAS data.
- The initial scan of the DAS and borehole geophones suggested the presence of three LPLD events: one at approximately 3000 s, close to formation breaking pressure, one at approximately 4200 s, and the last one at approximately 7000 s. Further analysis of the geophone data revealed that events on geophone data are swarms of MSEs and are not LPLDs. These MSEs may be accompanied by lower frequency LPLD events. Events at 7000 s seemed to have a source at the surface because of the reverse moveout from the surface toward the reservoir. In addition, surface seismograms suggest a local surface source close to FRAC1, which is closest to the wellpad.
- The low-frequency (0.1–5 Hz) DAS data suggested that the event at 3000 s is affected by injection noise. However, a surface seismic array recorded an event at approximately 3000 s on all three seismograms. The duration of the event is around a minute and has LPLD characteristics. The low-frequency (0.1–5 Hz) DAS data also revealed an event at approximately 4200 s. Unlike the 3000 s event, it is not visible on all DAS channels. It is also recorded by the surface seismic array three seismometers. We suggest that this event is likely an LPLD event as well.
- The DTS data show a warming effect in stage 9 during hydraulic fracture stimulation of stage 10. The temperature response appears to coincide with the LPLD events in the DAS spectrogram. This temperature change recorded by the DTS system likely suggests hydraulic connections between two consecutive stages, particularly due to the reactivation of preexisting fractures that triggered LPLD events.
- The instantaneous frequency of DAS data shows some temporal correlation with the DTS data in low frequencies. However, we show that low-frequency patches that are interpreted as LPLDs are accompanied with high microseismic activity. This could suggest that during stimulation of stage 10, preexisting fractures undergo shear failure and establish cross-stage flow that pushes back warmed fracturing fluid toward stage 9.
- Regional earthquakes are very unlikely to have any effect on the local temperature variation, as measured by DTS data. Thus, LPLD events observed in the current study in the DAS and surface seismic array and contemporaneous variation in temperature recorded by DTS are most likely related to local deformation in the reservoir during hydraulic fracturing rather than an overprint of a known or unknown regional earthquake in the distant area.

Acknowledgments

This research is funded through the U.S. DOE National Energy Technology Lab part of their Marcellus Shale Energy and Environmental Laboratory (MSEEL) (DOE award no. DE-FE0024297). We appreciate the Northeast Natural Energy LLC for providing data and technical support. We also thank S. Cole and two other anonymous reviewers for their constructive comments and help.

Data and materials availability

Data associated with this research are available and can be accessed via the following URL: http://mseel.org/.

References

Aki, K. T., 1969, Analysis of the seismic coda of local earthquakes as scattered waves: Journal of Geophysical Research, **74**, 615–631, doi: 10.1029/JB074i002p00615.

Aki, K. T., and B. Chouet, 1975, Origin of coda waves: Source, attenuation, and scattering effects: Journal of Geophysical Research, **80**, 3322–3342, doi: 10.1029/JB080i023p03322.

Boroumand, N., and D. W. Eaton, 2012, Comparing energy calculations: Hydraulic fracturing and microseismic monitoring: 74th Annual International Conference and Exhibition, EAGE, Extended Abstracts, doi: 10.3997/2214-4609.20148187.

Caffagni, E., D. Eaton, M. van der Baan, and J. P. Jones, 2015, Regional seismicity: A potential pitfall for identification of long-period long-duration events: Geophysics, **80**, no. 1, A1–A5, doi: 10.1190/geo2014-0382.1.

Das, I., and M. D. Zoback, 2011, Long-period, long-duration seismic events during hydraulic fracture stimulation of a shale gas reservoir: The Leading Edge, **30**, 778–786, doi: 10.1190/1.3609093.

Das, I., and M. D. Zoback, 2013a, Long-period, long-duration seismic events during hydraulic stimulation of shale and tight-gas reservoirs — Part 1: Waveform characteristics: Geophysics, **78**, no. 6, KS97–KS108, doi: 10.1190/geo2013-0164.1.

Das, I., and M. D. Zoback, 2013b, Long-period long-duration seismic events during hydraulic stimulation of shale and tight-gas reservoirs — Part 2: Location and mechanisms: Geophysics, **78**, no. 6, KS109–KS117, doi: 10.1190/geo2013-0165.1.

Eaton, D., M. van der Baan, J. B. Tary, B. Birkelo, N. Spriggs, S. Cutten, and K. Pike, 2013, Broadband microseismic observations from a Montney hydraulic fracture treatment, northeastern B.C., Canada: CSEG Recorder, **38**, 44–53.

Fisher, M. K., C. A. Wright, B. M. Davidson, A. K. Goodwin, E. O. Fielder, W. S. Buckler, and N. P. Steinsberger, 2005, Integrating fracture mapping technologies to improve stimulations in the Barnett shale: SPE Production and Facilities, **20**, 85–93, doi: 10.2118/77441-PA.

Fisher, T., and A. Guest, 2011, Shear and tensile earthquakes caused by fluid injection: Geophysical Research Letters, **38**, L05307.

Ghahfarokhi, P. K., T. Carr, L. Song, P. Shukla, and P. Pankaj, 2018, Seismic attributes application for the distributed acoustic sensing data for the Marcellus Shale: New insights to cross-stage flow communication: Presented at the SPE Hydraulic Fracturing Technology Conference and Exhibition, Paper 189888, doi: 10.2118/189888-MS.

Glasbergen, G., V. J. Yeager, R. P. Reyes, and D. M. Everett, 2010, Fluid-diversion monitoring: The key to treatment optimization: SPE Production and Operations, **25**, 262–274, doi: 10.2118/122353-PA.

Holley, E., and N. Kalia, 2015, Fiber-optic monitoring: Stimulation results from unconventional reservoirs: Presented at the Unconventional Resources Technology Conference, Paper 2151906.

Jin, G., and B. Roy, 2017, Hydraulic-fracture geometry characterization using low-frequency DAS signal: The Leading Edge, **36**, 975–980, doi: 10.1190/tle36120975.1.

Karaman, O. S., R. L. Kutlik, and E. L. Kluth, 1996, A field trial to test fiber optic sensors for downhole temperature and pressure measurements, West Coalinga Field, California: Presented at the SPE Western Regional Meeting, Paper 35685, doi: 10.2118/35685-MS.

Karrenbach, M., A. Ridge, S. Cole, K. Boone, D. Kahn, J. Rich, K. Silver, and D. Langton, 2017, DAS microseismic monitoring and integration with strain measurements in hydraulic fracture profiling: Presented at the Unconventional Resources Technology Conference, Paper 2670716.

Kavousi, P., T. Carr, T. Wilson, S. Amini, C. Wilson, M. Thomas, K. MacPhail, D. Crandall, B. J. Carney, I. Costello, and J. Hewitt, 2017, Correlating distributed acoustic sensing (DAS) to natural fracture intensity for the Marcellus shale: 87th Annual International Meeting, SEG, Expanded Abstracts, 5386–5390, doi: 10.1190/segam2017-17675576.1.

Kumar, A., E. V. Zorn, R. Hammack, and W. Harbert, 2017a, Seismic monitoring of hydraulic fracturing activity at the Marcellus shale energy and environment laboratory (MSEEL) Site, West Virginia: Presented at the Unconventional Resources Technology Conference, Paper 2670481.

Kumar, A., E. Zorn, R. Hammack, and W. Harbert, 2017b, Long-period, long-duration seismicity observed during hydraulic fracturing of the Marcellus Shale in Greene County, Pennsylvania: The Leading Edge, **36**, 580–587, doi: 10.1190/tle36070580.1.

Kumar, A, E. Zorn, R. Hammack, and W. Harbert, 2018, Long-period, long-duration seismic events and their probable role in reservoir stimulation and stage productivity: SPE, doi:10.2118/191377-PA.

Kwietniak, A., 2015, Detection of the long period long duration (LPLD) events in time- and frequency-domain: Acta Geophysica, **63**, 201–213, doi: 10.2478/s11600-014-0262-1.

Mitchell, C., J. Kurpan, and P. Snelling, 2013, Detecting long-period long-duration microseismic events during hydraulic fracturing in the Cline Shale Formation, West Texas: A case study: 83rd Annual International Meeting, SEG, Expanded Abstracts, 2233–2237, doi: 10.1190/segam2013-1416.1.

Montgomery, C. T., and M. B. Smith, 2010, Hydraulic fracturing: History of an enduring technology: Journal of Petroleum Technology, **62**, 26–40, doi: 10.2118/1210-0026-JPT.

Nadeau, R. M., and A. Guilhem, 2009, Nonvolcanic tremor evolution and the San Simeon and Parkfield, California, earthquakes: Science, **325**, 191–193, doi: 10.1126/science.1174155.

Obara, K., 2002, Nonvolcanic deep tremor associated with subduction in southwest Japan: Science, **296**, 1679–1681, doi: 10.1126/science.1070378.

Olofsson, B., and A. Martinez, 2017, Validation of DAS data integrity against standard geophones — DAS field test at Aquistore site: The Leading Edge, **36**, 981–986, doi: 10.1190/tle36120981.1.

Rahman, M., P. J. Zannitto, D. A. Reed, and M. E. Allan, 2011, Application of fiber-optic distributed temperature

sensing technology for monitoring injection profile in Belridge field, Diatomite reservoir: Presented at the SPE Digital Energy Conference and Exhibition, Paper 144116, doi: 10.2118/144116-MS.

Rutledge, J. T., and W. S. Phillips, 2003, Hydraulic stimulation of natural fractures as revealed by induced microearthquakes, Carthage Cotton valley gas field, East Texas: Geophysics, **68**, 441–452, doi: 10.1190/1.1567214.

Shelly, D. R., G. C. Beroza, S. Ide, and S. Nakamula, 2006, Low-frequency earthquakes in Shikoku, Japan, and their relationship to episodic tremor and slip: Nature, **442**, 188–191, doi: 10.1038/nature04931.

Sicking, C., J. Vermilye, P. Geiser, A. Lacazette, and L. Thompson, 2012, Permeability field imaging from microseismic: 82nd Annual International Meeting, SEG, Expanded Abstracts, doi: 10.1190/segam2012-1383.1.

Sierra, J. R., J. D. Kaura, D. Gualtieri, G. Glasbergen, D. Sarker, and D. Johnson, 2008, DTS monitoring of hydraulic fracturing: Experiences and lessons learned: Presented at the SPE Annual Technical Conference and Exhibition, Paper 116182, doi: 10.2118/116182-MS.

Tanimola, F., and D. Hill, 2009, Distributed fibre optic sensors for pipeline protection: Journal of Natural Gas Science and Engineering, **1**, 134–143, doi: 10.1016/j.jngse.2009.08.002.

Warpinski, N. R., J. Du, and U. Zimmer, 2012, Measurements of hydraulic-fracture-induced seismicity in gas shales: SPE Production and Operations, **27**, 240–252, doi: 10.2118/151597-PA.

Warpinski, N. R., S. L. Wolhart, and C. A. Wright, 2004, Analysis and prediction of microseismicity induced by hydraulic fracturing: Society of Petroleum Engineers Journal, **9**, 24–33.

Webster, P., M. Molenaar, and C. Perkins, 2016, DAS microseismic: CSEG Recorder, **41**, 38–39.

Wilson, T. H., T. Carr, B. J. Carney, M. Yates, K. MacPhail, A. Morales, I. Costello, J. Hewitt, E. Jordon, N. Uschner, M. Thomas, S. Akin, O. Magbagbeola, A. Johansen, L. Hogarth, O. Anifowoshe, and K. Naseem, 2018, Marcellus Shale model stimulation tests and microseismic response yield insights into mechanical properties and the reservoir discrete fracture network: Interpretation, **6**, no. 2, T231–T243, doi: 10.1190/INT-2016-0199.1.

Wilson, T. H., A. K. Hart, and P. Sullivan, 2016, Interrelationships of Marcellus Shale gas production to frac-induced microseismicity, interpreted minor faults and fractures zones, and stimulated reservoir volume, Greene County, Pennsylvania: Interpretation, **4**, no. 1, T15–T30, doi: 10.1190/INT-2015-0045.1.

Zecevic, M., G. Daniel, and D. Jurick, 2016, On the nature of long-period long-duration seismic events detected during hydraulic fracturing: Geophysics, **81**, no. 3, KS113–KS121, doi: 10.1190/geo2015-0524.1.

Zoback, M. D., A. Kohli, I. Das, and M. McClure, 2012, The importance of slow slip on faults during hydraulic fracturing stimulation of shale gas reservoirs: Presented at the SPE Americas Unconventional Resources Conference, Paper 155476, doi: 10.2118/155476-MS.

Biographies and photographs of the authors are not available.